Sensors and Materials, Vol. 37, No. 5 (2025) 1969–1975
MYU Tokyo

S & M 4034

Attempt to Impart Conductivity to Thallium Bromide by Thermal Diffusion Doping

Naoya Yamaishi,* Mikio Higuchi, Satoshi Yoshitake, and Junichi H. Kaneko

Graduate School of Engineering, Hokkaido University,
Kita 13 Nishi 8, Kita-ku, Sapporo, Hokkaido 060-8628, Japan

(Received February 10, 2025; accepted April 16, 2025)

Keywords: semiconductor, thallium bromide, radiation detector, gamma ray, polarization, doping

As part of the development of thallium bromide (TlBr) semiconductor detectors, impurity doping into TlBr by the thermal diffusion method was attempted, along with the exploration of ohmic electrodes. Dopant materials with ionic radii and valence similar to those of Tl or Br were selected. In TlBr samples of 1 mm thickness, Sr and Pb doping improved the leakage current by approximately 8 times compared with undoped samples under an applied voltage of −100 V. Various metal electrodes were formed on TlBr samples doped with Sr or Pb, and their *I*–*V* characteristics were evaluated. Rectifying properties were observed in the Pb-doped samples with Ti and In, as well as in the Sr-doped samples with Ti. These results suggest that Sr-doped TlBr and Ti may have potential for use as injection electrodes.

1. Introduction

Thallium bromide (TlBr) has high atomic number (Tl: 81, Br: 35) and density (7.56 g/cm^3), providing high detection efficiency for gamma rays and X-rays. Additionally, with a bandgap of 2.68 eV, it is expected to serve as a semiconductor detector without requiring liquid nitrogen cooling. TlBr also exhibits an electron mobility-lifetime product of 4×10^{-3} cm^2/V,(1) enabling a practical sensitive volume, and has demonstrated an energy resolution higher than 1%.(2) These characteristics make TlBr a promising material for applications in astrophysics, nuclear medical diagnostic devices such as positron emission tomography,(3) and nuclear security systems.(4)

In TlBr semiconductor detectors, performance degradation over time due to polarization caused by charge accumulation has been reported.(5) Two primary causes of polarization are considered: charge carrier trapping within the semiconductor bulk (6) and charge accumulation at the electrode–semiconductor interface.

The latter is attributed to the ionic conductivity of TlBr, where Tl$^+$ and Br$^-$ ions migrate to the electrodes, causing chemical changes in the electrodes.(7) On the basis of this mechanism, Hitomi *et al.* successfully achieved the continuous operation of TlBr semiconductor detectors by using Tl as the electrode material.(8) TlBr detectors with Tl electrodes operated continuously at room temperature for 1,000 h with a fixed polarity of applied voltage(9) and for tens of thousands

---

*Corresponding author: e-mail: smallboy0721@els.hokudai.ac.jp

https://doi.org/10.18494/SAM5588

ISSN 0914-4935
https://myukk.org/

of hours with alternating voltage polarity.(10) This method is explained by suppressing the reaction of Tl^+ and Br^- ions that reached the Tl electrodes.(8)

On the other hand, Leão and Lordi reported through simulations that polarization occurs much faster than the time it takes for Tl^+ and Br^- ions to reach the electrodes owing to ionic conduction.(11) This suggests that, apart from solving the electrode corrosion problem, the use of Tl and appropriate treatments likely resulted in the formation of a favorable ohmic contact, suppressing charge accumulation at the electrodes. However, Tl is toxic and highly susceptible to oxidation, posing handling challenges.

As an alternative to Tl electrodes, Datta *et al.* demonstrated the use of indium tin oxide (ITO) as an electrode material, achieving ohmic contact and enabling the continuous operation of TlBr semiconductor detectors for 4,000 h without alternating the applied voltage polarity.(12)

In this study, we attempted to dope TlBr by the thermal diffusion method to prevent charge accumulation at the TlBr–electrode interface. In previous studies on CdTe semiconductor detectors, doping methods were shown to achieve favorable ohmic contact.(13) Furthermore, the leakage current–voltage (*I*–*V*) characteristics of doped TlBr and various metal electrodes were systematically evaluated.

2. Experimental Procedure

2.1 Preparation of TlBr samples

TlBr powder with 99.99% purity was purified by the Bridgman–Stockbarger (BS) method at a rate of 5 mm/h, followed by 200 cycles of zone melting at a rate of 180 mm/h. Crystal growth by the BS method at a rate of 2.16 mm/h was then performed. The atmosphere during both purification and growth was HBr (18%) + N_2 (82%) at a pressure of 0.1 atm. TlBr crystals were grown in a quartz tube of 12 mm inner diameter, tapered at the tip to suppress nucleation. The samples were then cut to a thickness of 1 mm using a diamond disc saw, with hexane used as the coolant.

Doping elements were Sr, Pb, Ca, Ba, and S, which have similar valence and ionic radii to Tl and Br. The powdered Tl or Br compounds of the doping elements were pressed into Φ11 mm pellets, brought into contact with the TlBr wafers, and heated for 17 h in an $Ar+H_2$ atmosphere to induce thermal diffusion. The heating temperature was set to 50 °C lower than the melting point of TlBr or the doping material, whichever was lower, or to 180 °C. The diffusion of impurities into TlBr was evaluated using a secondary ion mass spectrometer (manufactured by ULVAC, PHI ADEPT1010).

For doped TlBr samples that exhibited clear conductivity, electrodes were formed on the sample surface as shown in Fig. 1. A Au electrode was placed at the center, surrounded by Au, Pt, Al, In, Cr, and Ti electrodes. Each electrode had a thickness of approximately 100 nm and an area of 3.14 mm^2. The electrodes were formed by the resistance heating method for Au, Al, and In, high-frequency sputtering for Cr, direct current sputtering for Pt, and electron beam evaporation for Ti.

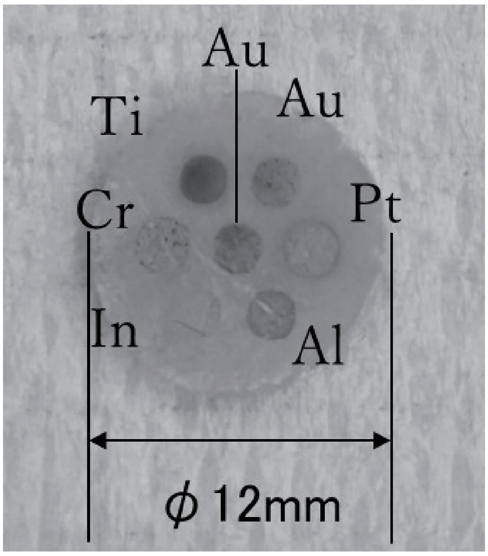

Fig. 1. Example of doped TlBr crystal sample with several metal electrodes.

2.2 Measurement method

The sheet resistance of the crystal was measured by a four-terminal method with a resistivity meter (K-705RS, manufactured by Kyowa Riken). A semiconductor probing system (HyBridge Co., Ltd.) was used to contact the crystal or electrodes fabricated on the crystal with tungsten probes at room temperature in an atmospheric environment. The *I*–*V* characteristics were evaluated in the ranges from 0 to 100 V and 0 to −100 V with steps of 0.5 V using a power device analyzer (Keysight B1505A).

3. Experimental Results and Discussion

3.1 Doping of TlBr

For all samples, the sheet resistance was above the measurement limit of 5.00 MΩ/□. Figure 2 shows examples of the *I*–*V* characteristics at room temperature for Sr-doped, Pb-doped, and undoped TlBr. For the Sr-doped sample, the average values from three different points on the same sample are shown, and for the Pb-doped sample, the average values from two different points are presented. Compared with the base TlBr, when a negative voltage was applied, samples doped with Sr exhibited five to eight times higher current, and Pb-doped samples showed approximately three times higher current at −100 V, although some variation was observed. No significant increase in current was observed for other doping materials.

For the samples with increased current, asymmetric *I*–*V* characteristics were consistently observed with good reproducibility, even though the same tungsten probe was used for both electrodes. This asymmetry could be due to the formation of a Schottky barrier at the interface between one of the tungsten probes and TlBr, possibly due to oxidation.

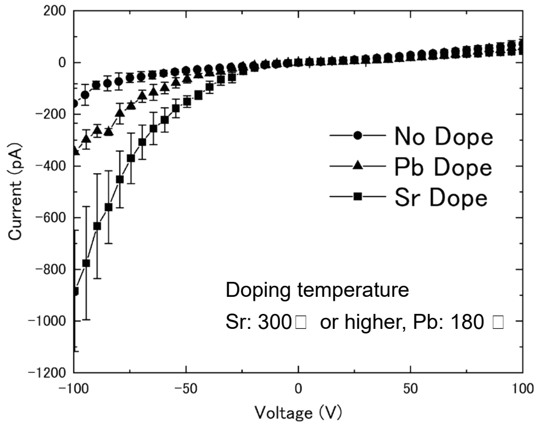

Fig. 2. Examples of measured *I–V* characteristics of TlBr with thermal diffusion of Sr and Pb. The cause of the rectification property is unknown.

Figure 3 shows the results of the secondary ion mass spectrometry analysis of Sr-doped and Pb-doped TlBr samples up to 10 μm from the surface, where a significant increase in current was observed. In the measurements, O_2^+ ions with an energy of 6.0 kV were used to scan an area of 25 × 18 μm² on the sample surface. On the basis of the ion intensity gradient, Sr is considered to have diffused up to 3 μm. The steep ion intensity gradient observed in the 0–0.5 μm region is considered to be due to residual Sr remaining on the surface. Sr detected at depths greater than 3 μm is considered to be an impurity retained within the crystal. Sr beyond this depth is considered to be a residual impurity within the crystal. Although Pb diffused up to 4 μm from the surface, the diffusion temperature was low at 180 °C compared with Sr's diffusion temperature higher than 300 °C, resulting in a significantly lower diffusion amount by one to two orders of magnitude.

Figure 4 shows the electric field dependence of the current density for the Sr-doped sample. The charge carriers in the semiconductor follow Eq. (1):

$$J_n = qn\mu_n E, \tag{1}$$

where J_n is the drift current density of conduction electrons, q is the elementary charge, n is the electron density, μ_n is the conduction electron mobility, and E is the electric field.

Figure 4 shows that the slope is different in the ranges from 0 to −5 V/mm and −5 to −15 V/mm, but the current density increases linearly, suggesting that drift current is the dominant conduction mechanism.

Table 1 shows the representative conduction mechanisms in the insulating film. In the electric field range from −15 to −25 V/mm in Fig. 4, the current density increases exponentially with the electric field strength, suggesting that ion conduction, hopping conduction, or a combination of both may be involved. Previous studies have pointed out that TlBr is an ion conductor,(14) and ions tend to diffuse via hopping.(15) By evaluating the temperature dependence of the leakage current, it is possible to identify the dominant mechanism, which will be a future task.

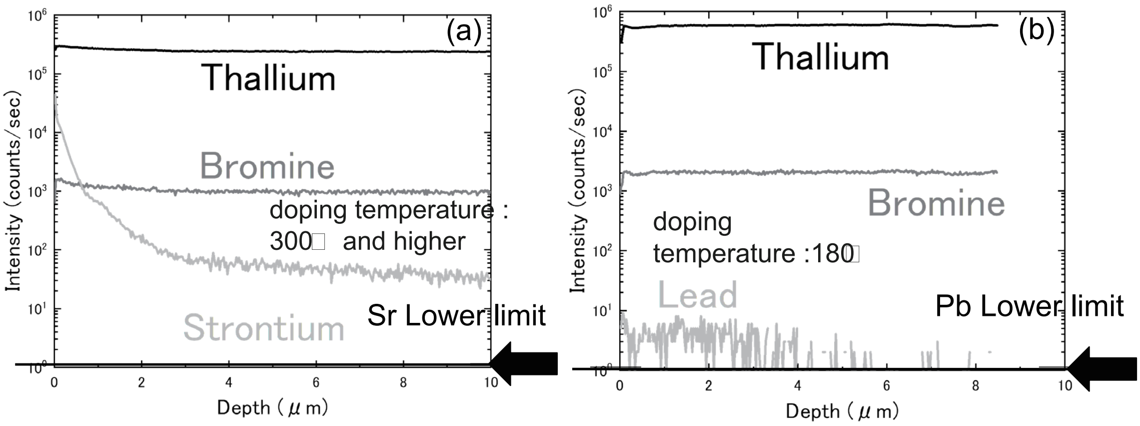

Fig. 3. Depth profis of (a) Sr and (b) Pb in TlBr.

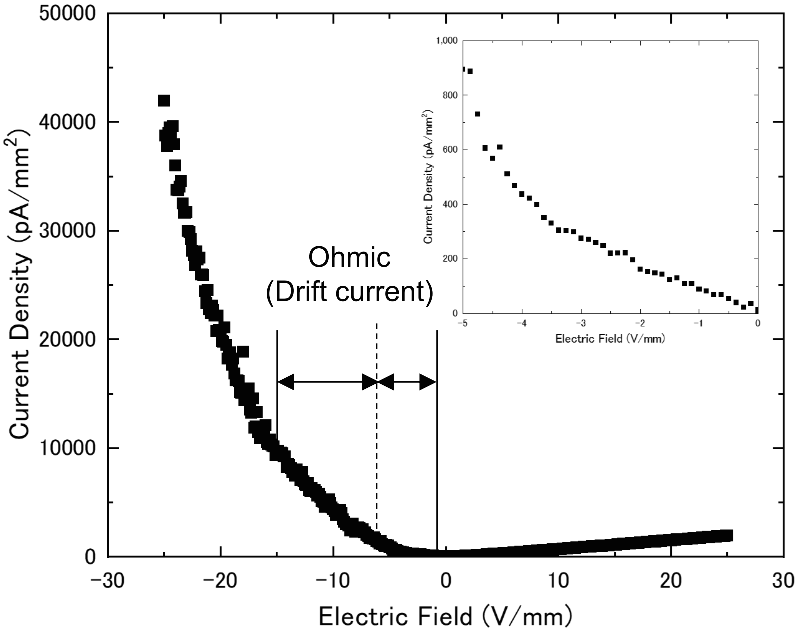

Fig. 4. Current densities of Sr-doped samples with different slopes from 0 to −5 V/mm and −5 to −15 V/mm, but drift currents predominate.

3.2 Measurement method

The *I–V* characteristics between Au and various metal electrodes placed on Pb-doped and Sr-doped TlBr are shown in Fig. 5. Approximately linear *I–V* characteristics were obtained for Au, Pt, Al, and Cr electrodes. In Pb-doped TlBr, In exhibited asymmetric rectifying characteristics, whereas in Sr-doped TlBr, Ti showed a similar behavior. Notably, in the case of Sr-doped TlBr with Au-Ti electrodes, leakage current was suppressed, resulting in *I–V* characteristics desirable for detector applications.

Table 1
Conduction processes in an insulator (temperature is constant).

Conduction Process	Expression
Schottky or Thermionic Emission(16)	$J = A^{*}T^{2}\exp\left[\frac{-q\left(\varphi_B - \sqrt{qE/4\pi\varepsilon_r\varepsilon_0}\right)}{kT}\right]$
Fowler–Nordheim Tunneling(16)	$J = \frac{q^3E^2}{8\pi hq\varphi_B}\exp\left[\frac{-8\pi(2qm_T^{*})^{\frac{1}{2}}}{3hE}\varphi_B^{3/2}\right]$
Poole–Frenkel Emission(16)	$J = q\mu N_c\exp\left[\frac{-q\left(\varphi_T - \sqrt{qE/\pi\varepsilon_i\varepsilon_0}\right)}{kT}\right]$
Hopping Conduction(17)	$J = qanv\exp\left(\frac{qaE}{kT} - \frac{E_a}{kT}\right)$
Ohmic Conduction(16)	$J = nq\mu E$, $n = N_c\exp\left[\frac{-\left(E_c - E_F\right)}{kT}\right]$
Space-charge-limited Conduction(16)	$J_{Ohm} = qn_0\mu\frac{V}{d}$, $J_{TFL} = \frac{9}{8}\mu\varepsilon\theta\frac{V^2}{d^3}$, $J_{Child} = \frac{9}{8}\mu\varepsilon\frac{V^2}{d^3}$
Ionic Conduction(16)	$J = J_0\exp\left[-\left(\frac{q\varphi_B}{kT} - \frac{Eqd}{kT}\right)\right]$

J: Current density, A^*: Effective Richardson constant, T: Absolute temperature, q: Elementary charge, $q\varphi_B$: Schottky barrier height, E: Electric field, k: Boltzmann's constant, ε_0: Vacuum permittivity, ε_r: Optical dielectric constant, h: Planck's constant, $m_T{}^*$: Tunneling effective mass in dielectric, μ: Electron mobility, N_c: Density of states in the conduction band, $q\varphi_T$: Trap energy level, a: Mean hopping distance, n: Electron concentration in the conduction band, v: Frequency of thermal vibration of electrons at trap sites, E_a: Activation energy, n_0: Concentration of free charge carriers in thermal equilibrium, V: Applied voltage, d: Thickness of thin film, ε: Static dielectric constant, θ: Ratio of the free carrier density to total carrier (free and trapped) density, J_0: Proportionality constant, d_I: Spacing of two nearby jumping sites.

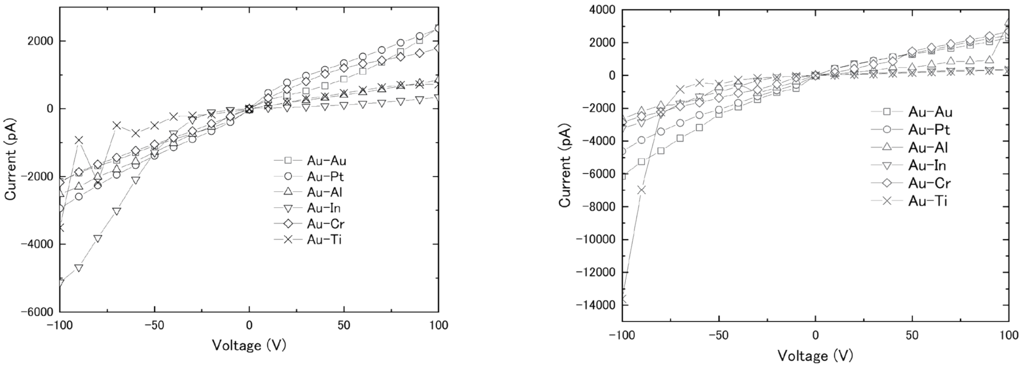

Fig. 5. I–V characteristics of Au and several metal electrodes on (a) Pb-doped and (b) Sr-doped TlBr.

In practice, since Au electrodes pose a corrosion issue, they cannot be used as they are. Therefore, further investigation is required regarding combinations with oxide metal electrodes such as ITO or the use of TiO_2.

4. Conclusions

In this study, the doping of TlBr crystals by a thermal diffusion method was attempted to reduce charge accumulation at the TlBr semiconductor–metal electrode interface. TlBr with 99.99% purity was used as the starting material. After purification by the BS method and zone melting, Sr, Pb, Ca, Ba, and S were doped into the TlBr polycrystal grown by the BS method. For TlBr samples doped with Sr or Pb, leakage currents three to eight times higher were observed at an applied voltage of −100 V compared with undoped TlBr samples. The conductive mechanism of TlBr samples doped with Sr and Pb may involve drift current, ionic conduction, and/or hopping conduction as the main contributions.

Various metal electrodes were formed on Sr-doped and Pb-doped TlBr samples, and the *I*–*V* characteristics between Au and various metal electrodes were evaluated. For Pb-doped TlBr, rectifying characteristics were observed for In, and for Sr-doped TlBr, rectification was observed for Ti. In particular, the Au-Ti electrode on Sr-doped TlBr exhibited leakage current suppressed by nearly three orders of magnitude in the reverse direction, providing suitable *I*–*V* characteristics for detector operation. On the other hand, since Au electrodes have corrosion issues, further validation of combinations with oxide metal electrodes such as ITO will be necessary in the future.

Acknowledgments

This work was supported by JSPS KAKENHI Grant Number JP21K12532.

References

1 K. Hitomi, N. Nagano, T. Onodera, S. Y. Kim, T. Ito, and K. Ishii: Nucl. Instrum. Methods Phys. Res., Sect. A **823** (2016) 15. https://doi.org/10.1016/j.nima.2016.03.107

2 H. Kim, A. Churilov, G. Ciampi, L. Cirignano, W. Higgins, S. Kim, P. O'Dougherty, F. Olschner, and K. Shah: Nucl. Instrum. Methods Phys. Res., Sect. A **629** (2011) 192. https://doi.org/10.1016/j.nima.2010.10.097

3 G. Ariño-Estrada, G. S. Mitchell, S. I. Kwon, J. Du, H. Kim, L. J. Cirignano, K. S. Shah, and S. R. Cherry: Phys. Med. Biol. **63** (2018) 04LT01. https://doi.org/10.1088/1361-6560/aaaa4e

4 P. M. Johns and J. C. Nino: J. Appl. Phys. **126** (2019) 040902. https://doi.org/10.1063/1.5091805

5 K. Hitomi, M. Matsumoto, O. Muroi, T. Shoji, and Y. Hiratate: IEEE Trans. Nucl. Sci. **49** (2002) 2526. https://doi.org/10.1109/TNS.2002.803851

6 H. L. Malm and M. Martini: IEEE Trans. Nucl. Sci. **21** (1974) 322. https://doi.org/10.1109/TNS.1974.4327478

7 V. Kozlov, M. Kemell, M. Vehkamäki, and M. Leskelä: Nucl. Instrum. Methods Phys. Res., Sect. A **576** (2007) 10. https://doi.org/10.1016/j.nima.2007.01.110

8 K. Hitomi, T. Shoji, and Y. Niizeki: Nucl. Instrum. Methods Phys. Res., Sect. A **585** (2008) 102. https://doi.org/10.1016/j.nima.2007.11.012

9 M. Nogami, K. Watanabe, and K. Hitomi: Jpn. J. Appl. Phys. **63** (2024) 096002. https://doi.org/10.35848/1347-4065/ad7803

10 A. Datta, J. Fiala, P. Becla, and S. Motakef: APL Mater. **5** (2017) 106109. https://doi.org/10.1063/1.5001181

11 C. R. Leão and V. Lordi: Phys. Rev. B: Condens. **87** (2013) 081202. https://doi.org/10.1103/PhysRevB.87.081202

12 A. Datta, P. Becla, and S. Motakef: Sci. Rep. **9** (2019) 9933. https://doi.org/10.1038/s41598-019-46360-z

13 Y. Hatanaka, M. Niraula, A. Nakamura, and T. Aoki: Appl. Surf. Sci. **175**–**176** (2001) 462. https://doi.org/10.1016/S0169-4332(01)00117-9

14 G. A. Samara: Phys. Rev. B: Condens. **23** (1981) 575. https://doi.org/10.1103/PhysRevB.23.575

15 A. Datta, P. Becla, and S. Motakef: Nucl. Instrum. Methods Phys. Res., Sect. A **784** (2015) 37. https://doi.org/10.1016/j.nima.2015.01.021

16 F.-C. Chiu: Adv. Mater. Sci. Eng. **2014** (2014) 578168, https://doi.org/10.1155/2014/578168

17 F.-C. Chiu, C.-Y Lee, and T.-Pan: J. Appl. Phys. **105** (2009) 074103. https://doi.org/10.1063/1.3103282